

3D phenomenological constitutive modeling of shape memory alloys based on microplane theory

This article has been downloaded from IOPscience. Please scroll down to see the full text article.

2013 Smart Mater. Struct. 22 025017

(<http://iopscience.iop.org/0964-1726/22/2/025017>)

View [the table of contents for this issue](#), or go to the [journal homepage](#) for more

Download details:

IP Address: 198.30.180.96

The article was downloaded on 10/01/2013 at 14:49

Please note that [terms and conditions apply](#).

3D phenomenological constitutive modeling of shape memory alloys based on microplane theory

R Mehrabi and M Kadkhodaei

Department of Mechanical Engineering, Isfahan University of Technology, Isfahan, 84156-83111, Iran

E-mail: kadkhodaei@cc.iut.ac.ir

Received 11 August 2012, in final form 13 November 2012

Published 9 January 2013

Online at stacks.iop.org/SMS/22/025017

Abstract

This paper concerns 3D phenomenological modeling of shape memory alloys using microplane theory. In the proposed approach, transformation is assumed to be the only source of inelastic strain in 1D constitutive laws considered for any generic plane passing through a material point. 3D constitutive equations are derived by generalizing the 1D equations using a homogenization technique. In the developed model, inelastic strain is explicitly stated in terms of the martensite volume fraction. To compare this approach with incremental constitutive models, such an available model is applied in its 1D integral form to the microplane formulation, and it is shown that both the approaches produce similar results for different uniaxial loadings. A nonproportional loading is then studied, and the results are compared with those obtained from an available model in which the inelastic strain is divided into two separate portions for transformation and reorientation. A good agreement is seen between the results of the two approaches, indicating the capability of the proposed microplane formulation in predicting reorientation phenomena in shape memory alloys. The results of the model are compared with available experimental results for a nonproportional loading path, and a good agreement is seen between the findings.

(Some figures may appear in colour only in the online journal)

1. Introduction

Shape memory alloys (SMAs) are one of the most popular smart materials, with the ability to release residual strain and return to their initial configuration when heated up to a particular temperature. Due to phase transformations during thermomechanical loading, the constitutive modeling of these materials is complex. The first models were phenomenological ones, describing superelastic 1D loadings (Tanaka 1986, Liang and Rogers 1997). Then, a new class of phenomenological models appeared based on a phase diagram and developed within a thermodynamic framework that was able to simulate more complex thermomechanical loading, such as the shape memory effect and heating/cooling under a constant stress (Brinson 1993, Boyd and Lagoudas 1996, LExcellent and Leclercq 1996, Bo and Lagoudas 1999a, Morin *et al* 2011). Most of the models developed in recent

years focus on different particular key points of SMAs, including tension–compression asymmetry (Raniecki and LExcellent 1998, Grabe and Bruhns 2009) and a description of internal loops and cycling effects (Tanaka *et al* 1995, Bo and Lagoudas 1999b, Lagoudas and Entchev 2004). The latest models were implemented in FEA packages and used to design devices with complex shapes under thermomechanical loading (Popov and Lagoudas 2007, Zaki and Moumni 2007, Hartl *et al* 2010, Mirzaeifar *et al* 2010, Oliveira *et al* 2010). Qidwai and Lagoudas (2000) proposed a Gibbs free energy function that takes the transformation hardening into account. Lagoudas *et al* (2012) developed return map algorithms for the numerical implementation of this model into a finite element program.

One of the main challenges in SMA modeling is satisfying the deviation from normality rule in the case of nonproportional loading, as shown by Lim and McDowell

(1999). Peng *et al* (2001) defined generalized equivalent stress and strain to be used in the constitutive equations of shape memory alloys for modeling SMA responses under nonproportional loading paths. Bouvet *et al* (2004) conducted several experiments on polycrystalline CuAlBe to investigate martensite reorientation in proportional and nonproportional loadings. They also proposed a non-associated flow rule corresponding to a phase transformation surface to assess the inelastic strain of the alloy. The phase transformation surface and the numerical values of coefficients in the model are obtained based on the behaviors observed in the experiments done on CuAlBe. This model can only predict the superelastic behavior of SMAs. Later, Saint Sulpice *et al* (2009, 2012) developed a 3D macroscopic model for the study of superelasticity in SMAs under cyclic multiaxial nonproportional loadings based on experimental works.

Another class of models for studying the behavior of SMAs under nonproportional loadings directly considers the martensite reorientation by dividing the inelastic strain into two different terms for transformation strain and reorientation strain. Panico and Brinson (2007) proposed a phenomenological model based on the thermodynamics of irreversible processes to investigate nonproportional multiaxial loadings. This model was able to evaluate the self-accommodated and oriented martensite. Furthermore, according to the loading direction, the reorientation of the product phase was considered. Arghavani *et al* (2010) studied SMA behaviors under general loadings at small and finite deformations. They proposed a constitutive model based on continuum thermodynamics with internal variables in which pure reorientation was decoupled from pure phase transformation in order to study the reorientation phenomena in nonproportional loadings.

In most of the existing three-dimensional phenomenological models, some of the material parameters cannot be directly evaluated and must be calibrated by comparing the obtained responses with experimental results. An alternative method for constitutive modeling of SMAs is based on microplane theory. In this approach, there is no separate expression for martensite reorientation, and all material parameters can be easily determined from uniaxial tension tests at different temperatures. The main idea in microplane theory is to consider a 1D model for some directions on selected planes, called microplanes, passing through any material point. Then, the integral form of the principle of complementary virtual work is employed to obtain 3D constitutive equations. Brocca *et al* (2002) suggested the application of microplane theory in SMA modeling, then Kadkhodaei *et al* (2007, 2008) developed this idea by proposing a model which was proved to satisfy deviation from normality. This model is able to simulate both the shape memory effect and superelasticity in shape memory alloys.

In this paper, first, the constitutive model based on microplane theory is proposed. A numerical procedure is then developed to implement the proposed model as a user material subroutine (UMAT) in the ABAQUS/Standard commercial code. Stress–strain diagrams for tensile and shear loadings as well as the strain–temperature response under a

constant axial stress are obtained using the present model and are compared those reported by Qidwai and Lagoudas (2000). The results obtained from the both approaches are shown to be in a very good agreement, indicating the capability of explicit microplane theory in employing 1D constitutive models to predict the behavior of shape memory alloys under various types of loading. The nonproportional tension–torsion loading–unloading path studied by Panico and Brinson (2007) is investigated by the microplane formulation, and a comparison of the results shows the capability of the proposed model in predicting reorientation phenomena under such loadings. Finally, for experimental validation, the nonproportional tensile stress–shear stress test studied by Sittner *et al* (1995) is investigated. The empirical findings are compared with the numerical results of the Panico and Brinson model and those of the present microplane formulation. The good agreement seen between the results indicates the reasonable accuracy of the proposed microplane approach in studying the SMA behaviors at different conditions.

In summary, this paper is organized as follows: section 2 addresses the formulation of the present microplane constitutive model, while section 3 compares the predictions of the microplane model in uniaxial loadings with the results shown by Qidwai and Lagoudas (2000). The Panico and Brinson model as well as the numerical simulations for comparison of the present model against theirs is presented in section 4. Experimental validation of the proposed model using the empirical findings of Sittner *et al* (1995) is done in section 5. Finally, some concluding remarks are provided in section 6.

2. Microplane formulation

Here a three-dimensional macroscopic constitutive model for SMAs based on microplane formulation is briefly explained. Referring to figure 1, for any microplane passing through a material point, the normal and shear stress vectors are obtained using the projection rule in the form:

$$\sigma_N = N_{ij}\sigma_{ij}, \quad N_{ij} = n_i n_j \quad (1)$$

$$\sigma_T = T_{ij}\sigma_{ij}, \quad T_{ij} = \frac{(n_i t_j + n_j t_i)}{2},$$

$$t_i = \frac{\sigma_{ik} n_k - \sigma_N n_i}{\sqrt{\sigma_{jr} \sigma_{js} n_r n_s - \sigma_N^2}} \quad (2)$$

where σ_N is normal stress, σ_T is shear stress, and n_i represents the components of the unit normal vector \mathbf{n} to the plane.

To obtain normal and shear strains on each microplane, 1D constitutive relations between the projected stresses and the corresponding strains are considered. Since the martensitic transformation is associated with shear deformations, the total inelastic strain is assumed to be only due to shear strains on the microplanes. So, only for the shear direction on each microplane, a 1D SMA constitutive law is used and a linear elastic stress–strain relation is considered for the normal direction. Considering the volumetric–deviatoric split for the

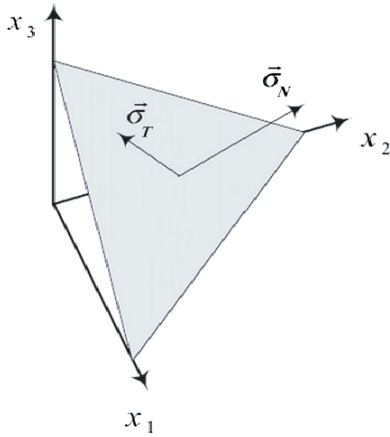


Figure 1. Stress components on a microplane (Kadkhodaei *et al* 2007).

normal stress as

$$\sigma_V = \frac{\delta_{ij}}{3} \sigma_{ij}, \quad \sigma_D = \sigma_N - \sigma_V = \left(n_i n_j - \frac{\delta_{ij}}{3} \right) \sigma_{ij} \quad (3)$$

the following local constitutive equations are assumed for the volumetric and the deviatoric parts of the normal strain as well as the elastic part of the shear strain

$$\begin{aligned} \varepsilon_V &= \frac{(1-2\nu)\sigma_V}{E(\xi)}, & \varepsilon_D^e &= \frac{(1+\nu)\sigma_D}{E(\xi)}, \\ \varepsilon_T^e &= \frac{(1+\nu)\sigma_T}{E(\xi)} \end{aligned} \quad (4)$$

in which ν is Poisson's ratio and E is Young's modulus, which is a function of ξ .

The effective elastic modulus is calculated in terms of the martensite volume fraction using the Reuss model for SMA behavior (Brinson and Huang 1996):

$$\frac{1}{E(\xi)} = \frac{(1-\xi)}{E_A} + \frac{\xi}{E_M} \quad (5)$$

where E_A and E_M are respectively the elastic moduli of pure austenite and pure martensite phases. To obtain the inelastic strain for shear directions, the 1D integral form of the Lagoudas constitutive equations is employed. The transformation shear strain is stated as

$$\varepsilon^{\text{tr}} = H \cdot \xi_\sigma(\bar{\sigma}, T) \quad (6)$$

in which H is the maximum recoverable strain and $\xi_\sigma(\bar{\sigma}, T)$ is the stress-induced martensite volume fraction, which may be expressed as a function of the effective stress, $\bar{\sigma}$, and temperature by means of a phenomenological relation.

The principle of complementary virtual work may be written as

$$\frac{4\pi}{3} \boldsymbol{\varepsilon} : \delta \boldsymbol{\sigma} = 2 \int_{\Omega} (\varepsilon_N \delta \sigma_N + \varepsilon_T \delta \sigma_T) d\Omega \quad (7)$$

where Ω is the surface of a unit hemisphere representing all possible orientations at a point. Substituting the relations (1), (2), (3), (4) and (6) into (7) and considering the independence of the components of the virtual stress tensor, the macroscopic

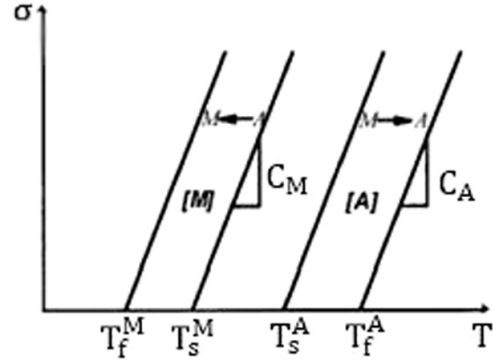


Figure 2. Stress-temperature phase diagram.

strain for any desired stress and temperature is explicitly obtained in the following form

$$\begin{aligned} \varepsilon_{ij} &= \varepsilon_{ij}^e + \varepsilon_{ij}^{\text{tr}} = -\frac{\nu}{E(\xi)} \sigma_{ss} \delta_{ij} \\ &+ \frac{1+\nu}{E(\xi)} \sigma_{rs} \cdot \frac{3}{2\pi} \int_{\Omega} (N_{rs} N_{ij} + T_{rs} T_{ij}) d\Omega \\ &+ H \cdot \xi_\sigma \cdot \frac{3}{2\pi} \int_{\Omega} T_{ij} d\Omega. \end{aligned} \quad (8)$$

3. Comparison between microplane formulation and Qidwai and Lagoudas (2000) model

In this section, the proposed approach is compared with Qidwai and Lagoudas (2000) model by employing the 1D form of their 3D constitutive equations. However, Qidwai and Lagoudas predict the martensite volume fraction by using an evolutionary equation, but explicit relationships suggested by Liang and Rogers (1997) are utilized in microplane model. Accordingly, in terms of the effective macroscopic stress acting on the material point at which the microplane is constructed, the stress-induced martensite volume fraction is stated as:

$$\begin{aligned} A \rightarrow M : \xi_\sigma &= \frac{1-\xi_0}{2} \cos \left[\frac{\pi}{T_s^M - T_f^M} \left(T - T_f^M - \frac{\bar{\sigma}}{C_M} \right) \right] \\ &+ \frac{1+\xi_0}{2}, \\ &\text{for } C_M(T - T_s^M) < \bar{\sigma} < C_M(T - T_f^M) \end{aligned} \quad (9)$$

$$\begin{aligned} M \rightarrow A : \xi_\sigma &= \frac{\xi_0}{2} \left\{ \cos \left[\frac{\pi}{T_f^A - T_s^A} \right. \right. \\ &\times \left. \left. \left(T - T_s^A - \frac{\bar{\sigma}}{C_A} \right) \right] + 1 \right\}, \\ &\text{for } C_A(T - T_f^A) < \bar{\sigma} < C_A(T - T_s^A). \end{aligned} \quad (10)$$

In these relations, ξ_0 is the martensite volume fraction prior to the current transformation, T_f^M , T_s^M , T_s^A , and T_f^A are transformation temperatures, and C_M and C_A are the slope of martensite and austenite strips in the stress-temperature phase diagram shown in figure 2. The regions in which forward and reverse transformations take place are shown in this figure.

Table 1. Material parameters of the constitutive model used from Qidwai and Lagoudas (2000) model.

Material constant	E_A (GPa)	E_M (GPa)	ν	H (%)	T_f^A (K)	T_s^A (K)	T_s^M (K)	T_f^M (K)	$C_A = C_M$ (MPa K ⁻¹)
Value	70	30	0.3	5	315	295	291	271	7

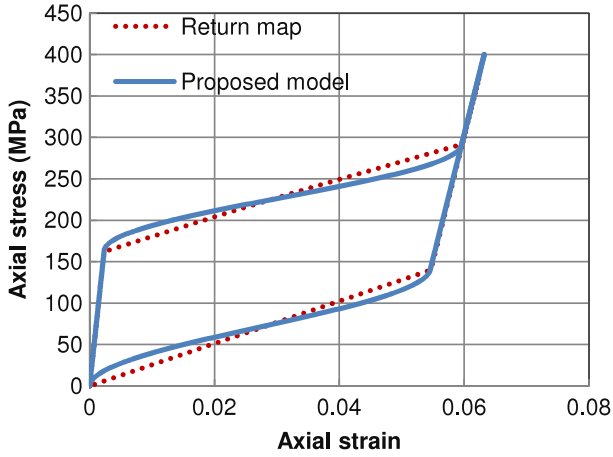
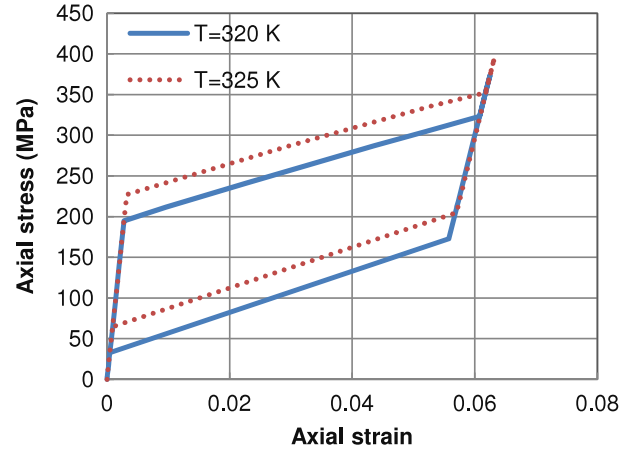


Figure 3. Superelastic behavior of SMA in a uniaxial state of stress at $T = T_f^A$.

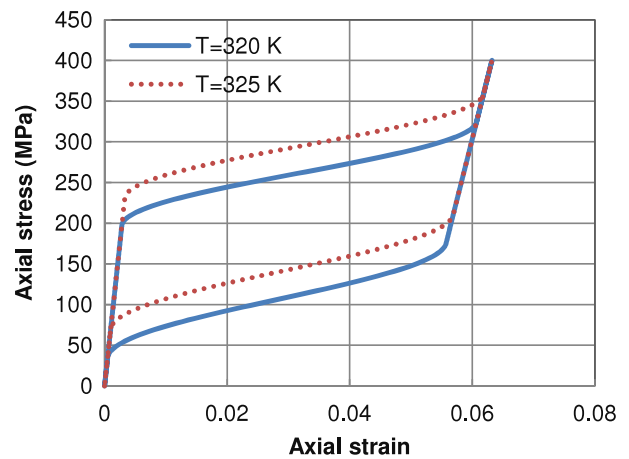
To obtain numerical results, the microplane equation (8) in conjunction with relations (9) and (10) are implemented as a UMAT for ABAQUS. The integrals are numerically calculated using the method proposed by Bazant and Oh (1986). The material parameters are given in table 1.

At first, a simple tensile loading–unloading at $T = T_f^A$ is simulated, and the corresponding stress–strain curves obtained using the microplane model and return mapping algorithm for the Lagoudas model are shown in figure 3. As this figure shows, the response obtained from the microplane formulation correlates quite well with that obtained from the model proposed by Lagoudas. The slight discrepancy between the results in the forward and reverse transformation regions is associated with the use of harmonic functions (9) and (10) in the microplane formulation, and more consistent results are obtained if a linear relation is utilized for ξ . Shown in figures 4(a) and (b) are stress–strain diagrams at two different temperatures above T_f^A . A comparison between these figures indicates that the proposed explicit microplane model can easily reproduce the results obtained from the implicit evolutionary equations proposed by Qidwai and Lagoudas (2000).

In order to show consistency between the two models at different conditions, strain–temperature response under the constant axial stress of 50 MPa is studied and shown in figure 5. The SMA is initially at a temperature below T_f^M in the full martensite phase while the dead load causes 5% strain. Then its temperature increases to above T_f^A so that full transformation from martensite to austenite is induced and the transformation strain is totally recovered. Cooling the alloy to below T_f^M again produces a 5% strain, and this cycle repeats upon cyclic heating–cooling of the SMA. It is seen that the results of the two approaches are very similar to each other.



(a)



(b)

Figure 4. Superelastic behavior of SMA in a uniaxial state of stress at two different temperatures: (a) Return mapping algorithm for the Lagoudas model and (b) microplane model.

Figure 6 shows a thin-walled SMA tube with a radius of 3 mm, thickness of 0.3 mm, and length of 50 mm subjected to torsion at one end while the other end is fixed. Figure 7 shows the shear stress–strain curve of this torque tube at temperature T_f^A . In this case, the maximum transformation strain H is taken to be 1% (Qidwai and Lagoudas 2000). As is seen, the proposed microplane model can predict the SMA behavior in torsion fairly well although 1D constitutive equations related to uniaxial response are utilized as the basic relations in deriving equation (8). The shear transformation strain in pure torsion should be $\sqrt{3}H\xi$ (Kadkhodaei *et al* 2008), and equation (8) yields the following result:

$$\gamma^{tr} = 2\varepsilon_{12}^{tr} = 2H\xi \times \frac{3}{2\pi} \int_{\Omega} T_{12}d\Omega = 2H\xi \times 0.895. \quad (11)$$

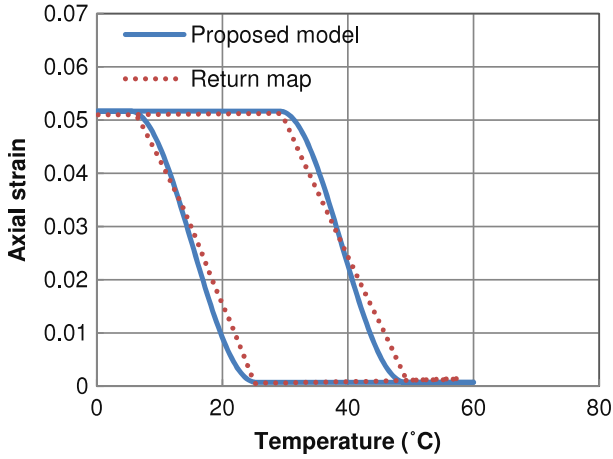


Figure 5. Strain–temperature hysteresis curve at a constant stress.

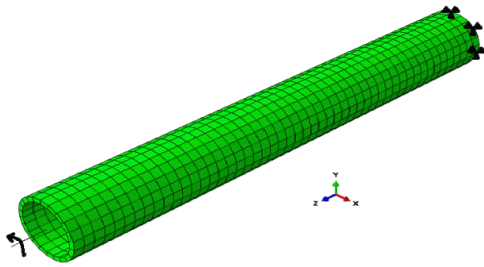


Figure 6. Schematic of the finite element model for a thin-walled tube under pure torsion.

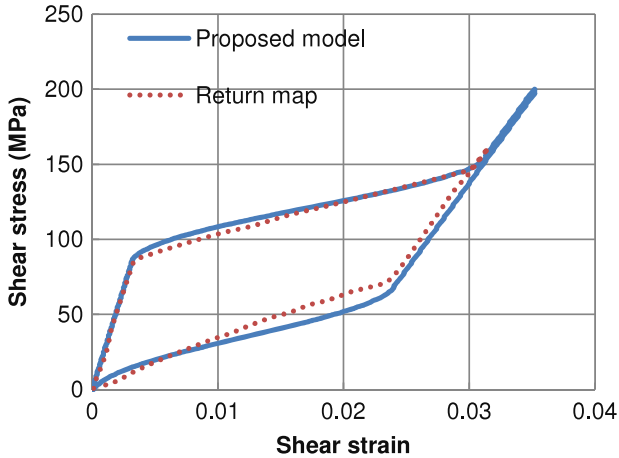


Figure 7. Shear stress–shear strain diagram of the SMA tube under pure torsion at $T = T_f^A$.

This means the existence of around 3.3% error in the microplane results which is due to errors in the numerical evaluation of the integrals.

The good agreement between the results of the microplane approach and the Qidwai and Lagoudas model indicates the following two major abilities of the proposed model:

- When 1D loadings are studied, microplane formulation gives the same results as if the 1D constitutive laws

were directly used although 1D constitutive laws for the normal and tangential directions of each microplane are not the same as those utilized in a directly macroscopic 1D constitutive model.

- The microplane model employs explicit constitutive equations and can be more easily utilized than implicit constitutive models.

After exhibiting the capabilities of the proposed microplane model in uniaxial loadings at various conditions, investigation of this model in some multiaxial loadings followed by experimental validation of the results are presented in the next sections.

4. Comparison between the microplane approach and Panico model under multiaxial loadings

When subjected to nonproportional multiaxial loadings, thermomechanical behaviors of an SMA are accompanied by martensite reorientation. As the SMA microplane model considers the possibility of martensitic transformation on several planes with different orientations, only the transformation strain is taken into account and no separate expression is attributed to reorientation in the inelastic part of strain. However, the proposed microplane approach is able to predict martensite reorientation in the 3D macroscopic response. To show this, the nonproportional loading path studied by Panico and Brinson (2007) is investigated by the microplane model as well, and the results are compared against each other.

Panico and Brinson (2007) proposed a model in which martensite reorientation is explicitly taken into account. The additive decomposition between elastic and inelastic strains is stated as:

$$\boldsymbol{\varepsilon} = \boldsymbol{\varepsilon}^e + \boldsymbol{\varepsilon}^{\text{in}}. \quad (12)$$

The increment of inelastic strain is divided into two portions, which originate from transformation of the parent phase and reorientation of previously developed oriented martensite:

$$\begin{aligned} \dot{\boldsymbol{\varepsilon}}^{\text{in}} &= \dot{\boldsymbol{\varepsilon}}^{\text{tr}} + \dot{\boldsymbol{\varepsilon}}^{\text{re}}, & \dot{\boldsymbol{\varepsilon}}^{\text{tr}} &= \dot{\lambda}_{\text{tr}} \mathbf{X}_{\text{tr}}, \\ \dot{\boldsymbol{\varepsilon}}^{\text{re}} &= \dot{\lambda}_{\text{re}} \hat{\mathbf{I}} : \mathbf{X}_{\text{re}} \end{aligned} \quad (13)$$

where $\dot{\lambda}_{\text{tr, re}}$ are positive Lagrange multipliers, and the fourth-order tensor $\hat{\mathbf{I}}$ is defined as:

$$\hat{\mathbf{I}} = (\mathbf{I}' - \mathbf{n} \otimes \mathbf{n}) \quad (14)$$

in which \mathbf{I}' is the fourth-order identity deviatoric tensor, $\mathbf{n} = \boldsymbol{\varepsilon}^{\text{in}} / \|\boldsymbol{\varepsilon}^{\text{in}}\|$, and \mathbf{X}_{tr} and \mathbf{X}_{re} are following thermodynamical dissipative forces:

$$\begin{aligned} \mathbf{X}_{\text{tr}} &= \boldsymbol{\sigma}' - \rho[(T\Delta\eta_0 - \Delta u_0) + H\xi_\sigma] \\ &\times \frac{\boldsymbol{\varepsilon}^{\text{in}}}{\sqrt{3/2}\gamma\|\boldsymbol{\varepsilon}^{\text{in}}\|}, & \mathbf{X}_{\text{re}} &= \underline{\boldsymbol{\sigma}}' \end{aligned} \quad (15)$$

where $\boldsymbol{\sigma}'$, ρ , η and u are deviatoric stress tensor, material density, the specific entropy, and the specific free energy, respectively. For brevity, the evolution equations of this model

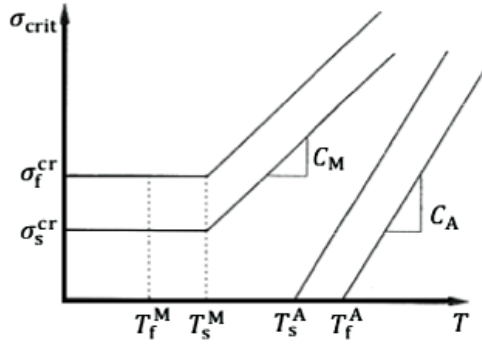


Figure 8. Critical stress–temperature phase diagram.

are not included in this paper and interested readers are referred to Panico and Brinson (2007).

Panico and Brinson utilized the phase diagram shown in figure 8. Accordingly, in order to be able to compare the results, the microplane equations in section 2 are used and the relationships suggested by Brinson (1993) are utilized for $\xi_\sigma(\bar{\sigma}, T)$. Referring to figure 8, the evolution equations for $\xi_\sigma(\bar{\sigma}, T)$ at different regions in the phase diagram are:

Conversion to Detwinned Martensite:

For $T > T_s^M$ and $\sigma_s^{cr} + C_M(T - T_s^M) < \bar{\sigma} < \sigma_f^{cr} + C_M(T - T_s^M)$:

$$\xi_\sigma = \frac{1 - \xi_{\sigma 0}}{2} \cos \left\{ \frac{\pi}{\sigma_s^{cr} - \sigma_f^{cr}} \times [\bar{\sigma} - \sigma_f^{cr} - C_M(T - T_s^M)] \right\} + \frac{1 + \xi_{\sigma 0}}{2}. \quad (16)$$

For $T < T_s^M$ and $\sigma_s^{cr} < \bar{\sigma} < \sigma_f^{cr}$:

$$\xi_\sigma = \frac{1 - \xi_{\sigma 0}}{2} \cos \left\{ \frac{\pi}{\sigma_s^{cr} - \sigma_f^{cr}} \times [\bar{\sigma} - \sigma_f^{cr}] \right\} + \frac{1 + \xi_{\sigma 0}}{2}. \quad (17)$$

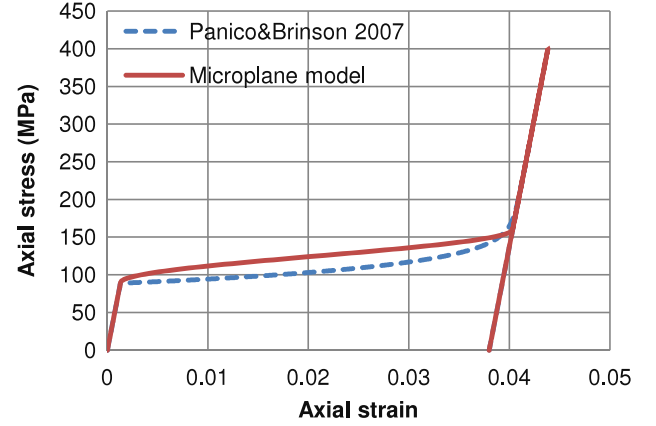
Conversion to Austenite: for $T > T_s^A$ and $C_A(T - T_f^A) < \bar{\sigma} < C_A(T - T_s^A)$:

$$\xi_\sigma = \frac{\xi_{\sigma 0}}{2} \left\{ 1 + \cos \left[\frac{\pi}{T_f^A - T_s^A} \left(T - T_s^A - \frac{\bar{\sigma}}{C_A} \right) \right] \right\} \quad (18)$$

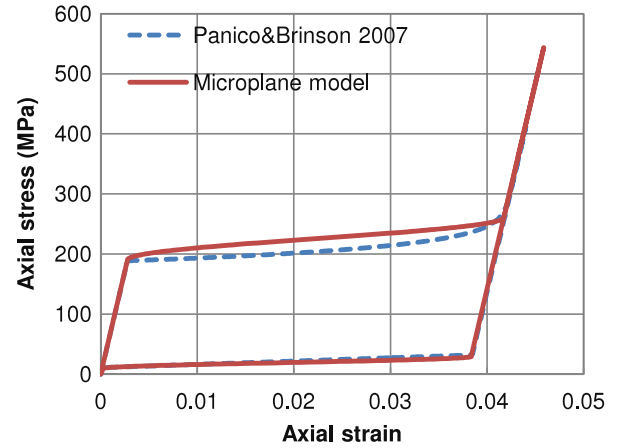
where $\xi_{\sigma 0}$ represents the detwinned martensite volume fraction prior to the current transformation.

At first, calibration is done to obtain the material parameters of microplane formulation based on those utilized by Panico and Brinson (2007). The values of these parameters are listed in table 2. To show the validity of these numbers, the uniaxial stress–strain responses obtained from the present microplane approach and Panico and Brinson model at three different temperatures are compared in figures 9(a)–(c). A good agreement is seen, indicating the reasonable accuracy of the obtained material parameters.

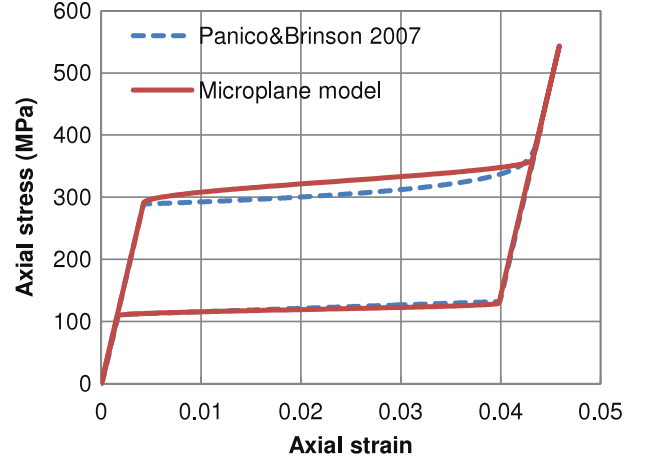
Shape memory effect at $T = 310$ K is considered in figure 10, and the present results are compared with those predicted by Panico and Brinson (2007). This figure shows



(a)



(b)



(c)

Figure 9. Numerical simulations of quasi plastic and superelasticity at different temperatures: (a) $T = 310$ K, (b) $T = 320$ K and (c) $T = 330$ K.

the ability of the proposed microplane model in predicting heating recovery after the removal of stress. As is seen, the two models produce very similar results in predicting the superelasticity and shape memory effect for 1D loading conditions.

After material parameters identification, in order to investigate martensite reorientation, the nonproportional

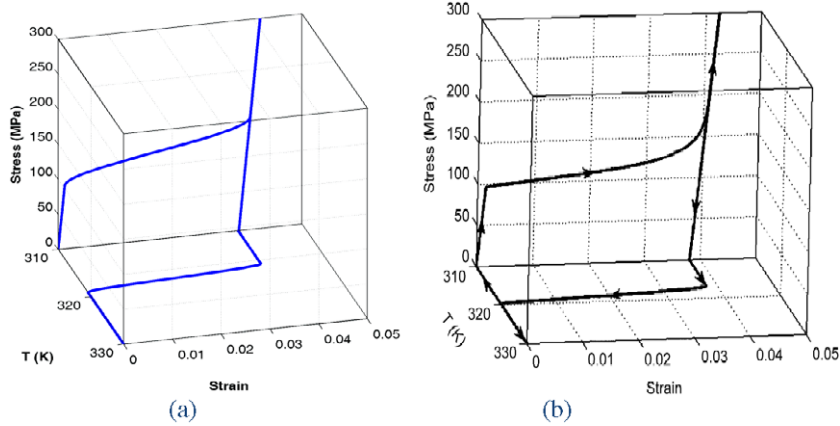


Figure 10. Numerical simulation of shape memory effect at $T = 310$ K: (a) microplane model, (b) Panico and Brinson (2007) model (reused from Panico and Brinson (2007), copyright 2007, with permission from Elsevier).

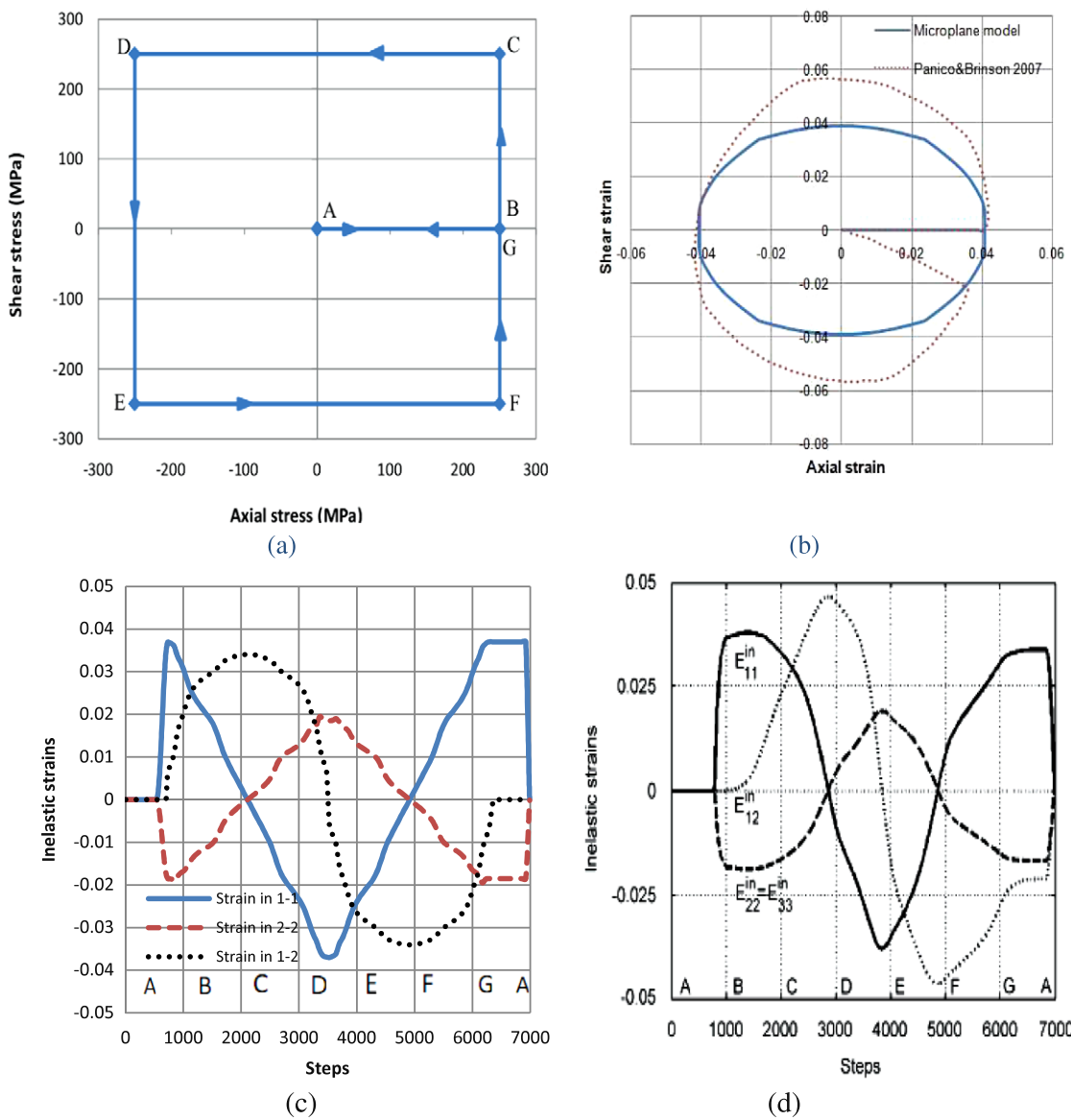


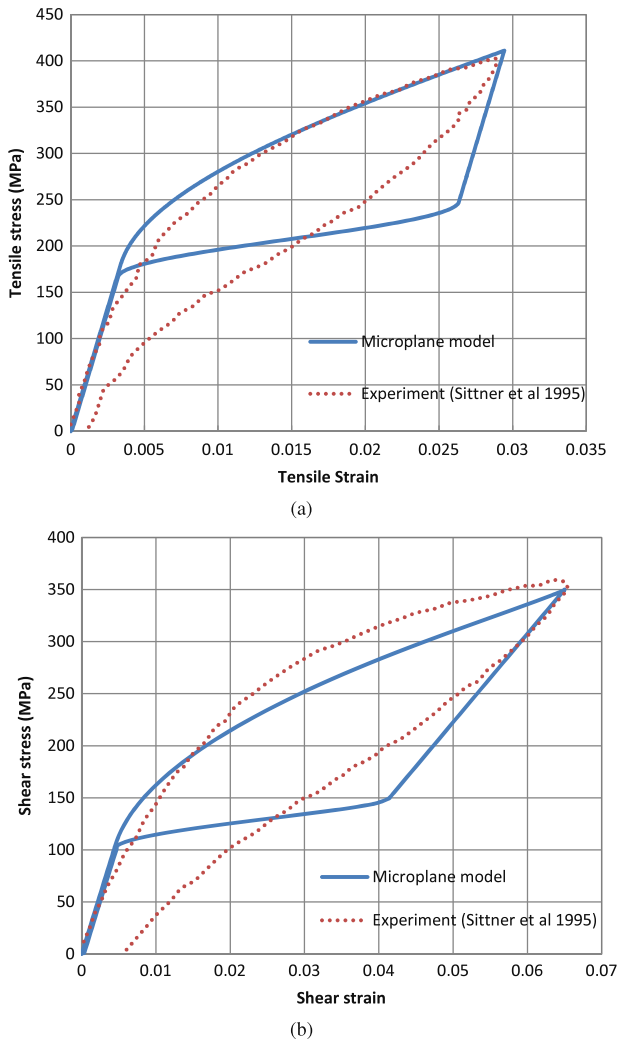
Figure 11. Nonproportional loading at $T = 320$ K: (a) axial stress–shear stress path, (b) axial strain–shear strain response, (c) inelastic strains for different loading stages in the microplane model and (d) corresponding results in the Panico and Brinson model (2007) (reused from Panico and Brinson (2007), copyright 2007, with permission from Elsevier).

Table 2. Material parameters of the constitutive model calibrated from the Panico and Brinson (2007) model.

Material constant	E (GPa)	σ_s^{cr} (MPa)	σ_f^{cr} (MPa)	ν	H (%)	T_f^A (K)	T_s^A (K)	T_s^M (K)	T_f^M (K)	$C_A = C_M$ (MPa K ⁻¹)
Value	68.4	90	160	0.36	3.8	319	317	310	306	10

Table 3. Material parameters of the constitutive model for CuAlZnMn calibrated from Sittner *et al* (1995) experiments.

Material constant	E (GPa)	σ_s^{cr} (MPa)	σ_f^{cr} (MPa)	ν	H (%)	T_f^A (K)	T_s^A (K)	T_s^M (K)	T_f^M (K)	C_A (MPa K ⁻¹)	C_M (MPa K ⁻¹)
Value	30	88	585	0.3	49	260	248	239	223	6.7	2

**Figure 12.** Responses of CuAlZnMn under uniaxial loading at $T = 285$ K: (a) tensile stress–strain and (b) shear stress–strain.

loading simulated by Panico and Brinson (2007) at 320 K is studied in figure 11. According to figure 11(a), a square-shaped path of axial stress–shear stress loading–unloading is considered. The amounts of the applied stresses are such that the material fully transforms to oriented martensite during the axial loading AB, and the entire subsequent parts of the loading involve only reorientation of the product phase.

Figure 11(b) shows the corresponding axial strain–shear strain response obtained from the two approaches. Although small differences are seen between the numerical results, the proposed microplane model can describe the reorientation phenomenon in SMAs under nonproportional loadings in a good qualitative manner. However, since there are no experimental results regarding this response, some thorough investigations are needed in future studies.

Figures 11(c) and (d) respectively show variations of the inelastic strain components at different stages of the loading–unloading path obtained from the microplane approach and from Panico and Brinson (2007). These results indicate coupling between the inelastic axial and shear strains which has been experimentally observed in nonproportional loadings of SMAs. For instance, within the loading path BC, where the shear stress is increased and the axial stress is held constant, an increase in the shear strain but a decrease in the axial strain is seen. During the unloading path CD, the axial stress is decreased to zero and further to compression with a constant amount of shear stress. 1D constitutive models cannot study these behaviors in multiaxial loadings, but the proposed approach is able to predict such responses, although only 1D constitutive laws are employed for each microplane. In fact, in any multiaxial loading, a combination of all the involved stress components leads to the individual strain components since ξ_σ is considered as a function of the effective stress and the components of the tensor \mathbf{T} depend on the amount of all the stress components according to equation (2). It should be noted that the inelastic strains are completely recovered upon unloading since the temperature is above T_f^A , and this indicates that the proposed approach is able to model superelasticity in a biaxial loading–unloading path.

The maximum recoverable strain in this case is $H = 0.38$, and it is seen in figure 11(c) that the amount of ε_{11}^{tr} is 0.38 at the end of loading path AB, meaning the completeness of the forward transformation. However, when the load direction is changed by applying shear stress in BC, ε_{11}^{tr} still evolves along with changes in the shear strain. This shows that the model is giving inelastic strains due to martensite reorientation since no more inelastic strain due to the transformation is expected. From the theoretical point of

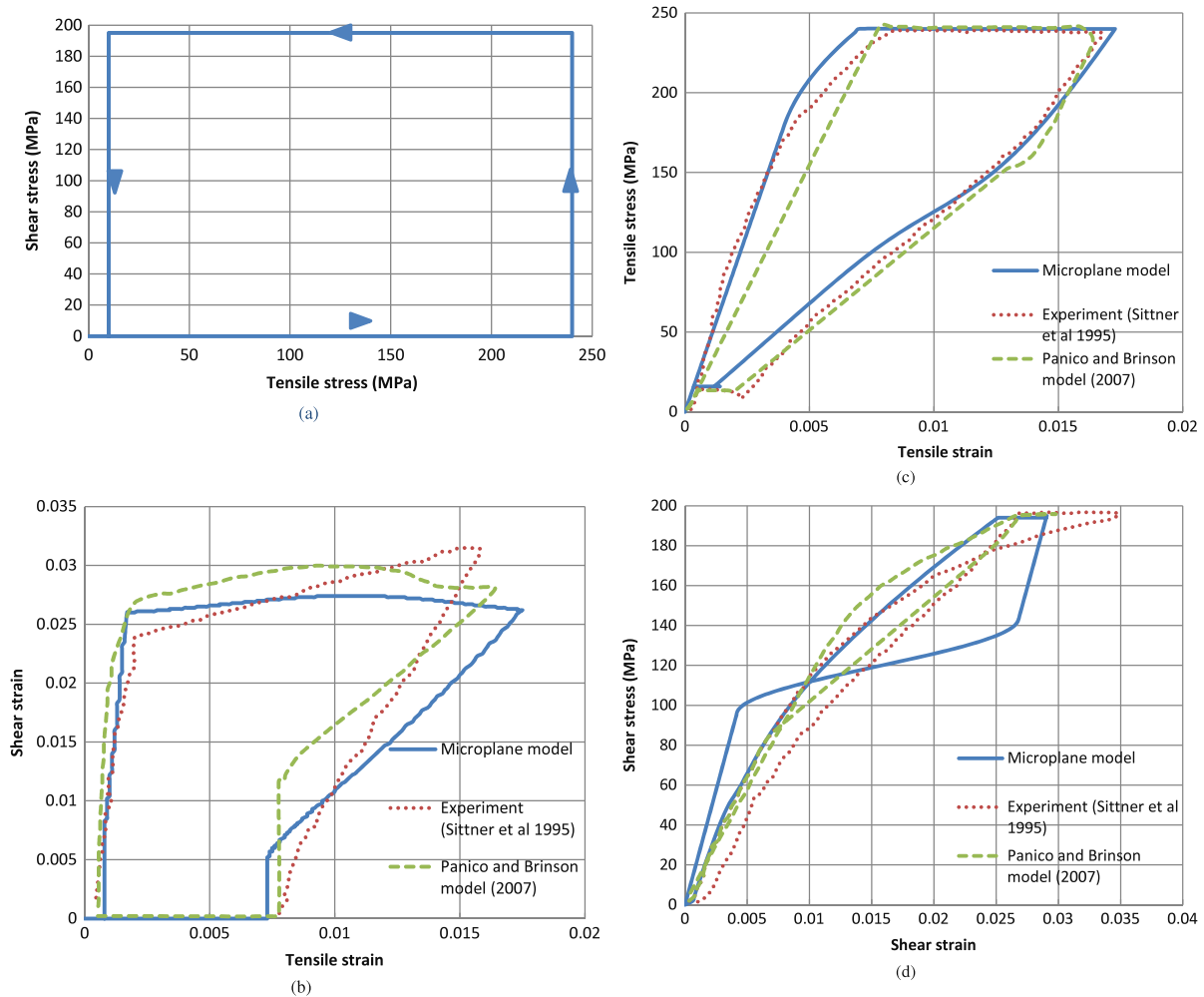


Figure 13. Comparison between the experimental and numerical results for a nonproportional multiaxial loading at $T = 285$ K: (a) Tensile stress–shear stress loading–unloading path. (b) Shear strain–tensile strain diagram. (c) Tensile stress–strain diagram. (d) Shear stress–strain diagram.

view, the last expression on the right hand side of equation (8) equals the inelastic strain. Accordingly, a multiplication of ξ_σ and $\int_\Omega T_{ij}d\Omega$ produces the inelastic strain, and the integral itself may evolve for a fixed amount of martensite volume fraction. In other words, this integral may be attributed to the portion of inelastic strain due to reorientation. This statement coincides with what is considered by Arghavani *et al* (2010) who decompose the inelastic strain rate into two portions: one for pure transformation and another for pure reorientation. Therefore, although only transformation is considered in the 1D constitutive laws, the reorientation phenomena can be captured with the use of the proposed microplane approach because the resultant of all the transformation strains in tangential directions on all microplanes passing through a material point gives rise to the whole macroscopic inelastic strain of that point.

5. Comparison with experimental results

To show the validity of the obtained results from the present microplane approach, the experimental findings reported by

Sittner *et al* (1995) are utilized, which have been widely used in previous models (Panico and Brinson 2007, Arghavani *et al* 2010, Lagoudas *et al* 2012). These experimental results belong to a nonproportional combination of tension–torsion loadings on a polycrystalline thin-walled tube fabricated from CuAlZnMn. Material parameters, provided in table 3, are obtained from the calibration of stress–strain responses for pure tension and pure torsion. A comparison between the experimental data and simulation results using these material parameters for pure tension and pure torsion are shown in figure 12. All simulations are performed at a temperature of $T = 285$ K, in agreement with the experiments.

Figure 13(a) shows the rectangular tensile–shear loading path studied by Sittner *et al* (1995). As is seen, the axial stress is first applied; then the shear stress is applied while the axial stress is constant. Afterwards, the tension and the shear stresses are respectively removed. The reported experimental findings, the numerical results presented by Panico and Brinson (2007), and those obtained by the proposed microplane approach for shear strain–tensile strain, tensile stress–strain, and shear stress–strain are respectively compared in figures 13(b)–(d). A reasonable similarity is

seen between the results, indicating the ability of the present model in reproducing the main characteristics of shape memory alloys under nonproportional loadings shown in the experiments.

6. Conclusions

In this study, a constitutive model is proposed for shape memory alloys based on microplane theory. 1D constitutive laws are considered for any generic plane passing through a material point and are generalized to 3D equations using a homogenization technique. The inelastic strain is explicitly stated in terms of the martensite volume fraction, and comparison of the results with those obtained by the incremental model of Qidwai and Lagoudas (2000) indicates the effectiveness of the present approach. It is also shown that, if a 1D macroscopic constitutive model is applied in microplane formulation, the results of that model is reproduced in uniaxial loadings. The nonproportional loading investigated by Panico and Brinson (2007) is further studied by the proposed approach, and a good agreement is shown to be between the results obtained from the two models. In the nonproportional loading case, the amounts of the applied stresses are such that the material fully transforms to oriented martensite during the first axial loading, and the whole subsequent parts of the loading only involve reorientation of the martensite. This indicates that microplane theory is able to take martensite reorientation into account although no separate expression corresponding to reorientation is considered in the fundamental 1D constitutive equations. The empirical findings for a nonproportional tensile stress–shear stress loading–unloading reported by Sittner *et al* (1995) are compared with the numerical results obtained from Panico and Brinson (2007) and those from the present approach. The good agreement seen between the findings show the capability of the microplane model in studying the behaviors of shape memory alloys under general multiaxial loadings although only 1D constitutive laws are utilized in the microplane formulation. The simple construction of this approach is very beneficial in determining the necessary material parameters as well.

References

- Arghavani J, Auricchio F, Naghdabadi R, Reali A and Sohrabpour S 2010 A 3D phenomenological constitutive model for shape memory alloys under multiaxial loadings *Int. J. Plast.* **26** 976–91
- Bazant Z P and Oh B H 1986 Efficient numerical integration on the surface of a sphere *ZAMM Z. Angew. Math. Mech.* **66** 37–49
- Bo Z and Lagoudas D C 1999a Thermomechanical modeling of polycrystalline SMAs under cyclic loading. Part I: theoretical derivations *Int. J. Eng. Sci.* **37** 1089–140
- Bo Z and Lagoudas D C 1999b Thermomechanical modeling of polycrystalline SMAs under cyclic loading. Part IV: modeling of minor hysteresis loops *Int. J. Eng. Sci.* **37** 1205–49
- Bouvet C, Calloch S and Lexcellent C 2004 A phenomenological model for pseudoelasticity of shape memory alloys under multiaxial proportional and nonproportional loadings *Eur. J. Mech. A Solids* **23** 37–61
- Boyd J and Lagoudas D C 1996 A thermodynamical constitutive model for shape memory materials. Part I: the monolithic shape memory alloy *Int. J. Plast.* **12** 805–42
- Brinson L C 1993 One dimensional constitutive behavior of shape memory alloys: thermomechanical derivation with non constant material functions *J. Intell. Mater. Syst. Struct.* **4** 229–42
- Brinson L C and Huang M S 1996 Simplifications and comparisons of shape memory alloy constitutive models *J. Intell. Mater. Syst. Struct.* **7** 108–14
- Brocca M, Brinson L C and Bazant Z 2002 Three-dimensional constitutive model for shape memory alloys based on microplane model *J. Mech. Phys. Solids* **50** 1051–77
- Grabe C and Bruhns O T 2009 Path dependence and multiaxial behavior of a polycrystalline NiTi alloy within the pseudoelastic and pseudoplastic temperature regimes *Int. J. Plast.* **25** 513–45
- Hartl D, Mooney J, Lagoudas D C, Calkins F and Mabe J 2010 Use of a Ni60Ti shape memory alloy for active jet engine chevron application: II. Experimentally validated numerical analysis *Smart Mater. Struct.* **19** 15–21
- Kadkhodaei M, Salimi M, Rajapakse R K N D and Mahzoon M 2007 Microplane modelling of shape memory alloys *Phys. Scr. T* **129** 329–34
- Kadkhodaei M, Salimi M, Rajapakse R K N D and Mahzoon M 2008 Modeling of shape memory alloys based on Microplane theory *J. Intell. Mater. Syst. Struct.* **19** 541–50
- Lagoudas D C and Entchev P 2004 Modeling of transformation-induced plasticity and its effect on the behavior of porous shape memory alloys. Part I: constitutive model for fully dense SMAs *Mech. Mater.* **36** 865–92
- Lagoudas D C, Hartl D, Chemisky Y, Machado L and Popov P 2012 Constitutive model for the numerical analysis of phase transformation in polycrystalline shape memory alloys *Int. J. Plast.* **32–33** 155–83
- Lexcellent C and Leclercq S 1996 A general macroscopic description of the thermomechanical behavior of shape memory alloys *J. Mech. Phys. Solids* **44** 953–80
- Liang C and Rogers C A 1997 One-dimensional thermomechanical constitutive relations for shape memory materials *J. Intell. Mater. Syst. Struct.* **8** 285–302
- Lim T J and McDowell D L 1999 Mechanical behavior of a Ni–Ti shape memory alloy under axial-torsional proportional and nonproportional loading *J. Eng. Mater. Technol.* **121** 9–18
- Mirzaeifar R, DesRoches R and Yavari A 2010 Exact solutions for pure torsion of shape memory alloy circular bars *Mech. Mater.* **42** 797–806
- Morin C, Moumni Z and Zaki W 2011 A constitutive model for shape memory alloys accounting for thermomechanical coupling *Int. J. Plast.* **27** 748–67
- Oliveira S A, Savi M A and Kalamkarov A L 2010 A three-dimensional constitutive model for shape memory alloys *Arch. Appl. Mech.* **18** 1163–75
- Panico M and Brinson L C 2007 A three-dimensional phenomenological model for martensite reorientation in shape memory alloys *J. Mech. Phys. Solids* **55** 2491–511
- Peng X, Yang Y and Huang S 2001 A comprehensive description for shape memory alloys with a two-phase constitutive model *Int. J. Solids Struct.* **38** 6925–40
- Popov P and Lagoudas D C 2007 A 3D constitutive model for shape memory alloys incorporating pseudoelasticity and detwinning of self-accommodated martensite *Int. J. Plast.* **23** 1679–720
- Qidwai M A and Lagoudas D C 2000 Numerical implementation of a shape memory alloy thermomechanical constitutive model

- using return mapping algorithm *Int. J. Numer. Methods Eng.* **47** 1123–68
- Raniecki B and Lexcellent C 1998 Thermodynamics of isotropic pseudoelasticity in shape memory alloys *Eur. J. Mech. A Solids* **17** 185–205
- Saint Sulpice L, Arbab Chirani S and Calloch S 2009 A 3D super-elastic model for shape memory alloys taking into account progressive strain under cyclic loadings *Mech. Mater.* **41** 12–26
- Saint Sulpice L, Arbab Chirani S and Calloch S 2012 Thermomechanical cyclic behavior modeling of Cu–Al–Be SMA materials and structures *Int. J. Solids Struct.* **49** 1088–102
- Sittner P, Hara Y and Tokuda M 1995 Experimental study on the thermoelastic martensitic transformation in shape memory alloy polycrystal induced by combined external forces *Metall. Mater. Trans. A* **26** 2923–35
- Tanaka K 1986 A thermomechanical sketch of shape memory effect: one dimensional tensile behavior *Res Mech.* **18** 251–63
- Tanaka K, Nishimura F, Hayashi T, Tobushi H and Lexcellent C 1995 Phenomenological analysis on sub loops and cyclic behavior in shape memory alloys under mechanical and/or thermal loads *Mech. Mater.* **19** 281–92
- Zaki W and Moumni Z 2007 A three-dimensional model of the thermomechanical behavior of shape memory alloys *J. Mech. Phys. Solids* **55** 2455–90